Journal of Quantitative Spectroscopy & Radiative Transfer 113 (2012) 1536–1546

Contents lists available at SciVerse ScienceDirect

Journal of Quantitative Spectroscopy & Radiative Transfer

journal homepage: www.elsevier.com/locate/jqsrt

Semiclassical calculations of half-widths and line shifts for transitions in the 30012←00001 and 30013←00001 bands of CO_2. III: Self collisions

Julien Lamouroux [a,b], Robert R. Gamache [a,b,*], Anne L. Laraia [a,b], Jean-Michel Hartmann [c], Christian Boulet [d]

[a] University of Massachusetts, School of Marine Sciences, 1 University Avenue, Lowell, MA 01854-5045, United States
[b] Department of Environmental, Earth, and Atmospheric Sciences, University of Massachusetts Lowell, 1 University Avenue, Lowell, MA 01854-5045, United States
[c] Laboratoire Interuniversitaire des Systèmes Atmosphériques, CNRS (UMR 7583), Université Paris Est Créteil, Université Paris Diderot, Institut Pierre-Simon Laplace, Université Paris Est Créteil, 94010 Créteil Cedex, France
[d] Institut des Sciences Moléculaires d'Orsay (ISMO;UMR 8214), CNRS, Université Paris-Sud, Bat. 350, Campus d'ORSAY, 91405 ORSAY Cedex, France

ARTICLE INFO

Article history:
Received 9 February 2012
Received in revised form
28 March 2012
Accepted 29 March 2012
Available online 14 April 2012

Keywords:
CO_2–CO_2
Half-width
Line shift
Temperature dependence of the half-widths
Venus
Mars

ABSTRACT

This paper is the third in a series devoted to accurate semi-empirical calculations of pressure-broadened half-widths, pressure-induced line shifts, and the temperature dependence of the half-widths of carbon dioxide. In this work complex Robert–Bonamy (CRB) calculations were made for transitions in two of the Fermi-tetrad bands for self-collisions, i.e. the CO_2–CO_2 system. The intermolecular potential (IP) was adjusted to match measurements of the half-width, its temperature dependence, and the line shift. It is shown that small changes in the parameters describing the IP lead to noticeable changes in the line shape parameters and that it is possible to find a set of IP parameters, which, when used in the CRB formalism, yield half-widths, their temperature dependence, and line shifts in excellent agreement with measurement. This work demonstrates that this agreement can be obtained if the atom–atom potential is expanded to high *order* and *rank* (here 20 4 4), the real and imaginary (S_1 and $Im(S_2)$) components are retained, and the determination of the trajectories is made by solving Hamilton's equations. It was found that the temperature dependence of the half-width is sensitive to the range of temperatures used in the fit and that the vibrational dependence of the line shape parameters for these two bands is very small. Databases of the half-width, its temperature dependence, and the line shift for the atmospheres of Venus (296–700 K fit range for the temperature exponents of the half-widths) and Mars (125–296 K fit range for the temperature exponents of the half-widths) are provided. The calculations are compared with the measured data for the bands under study.

1. Introduction

This work is the third in a series of studies devoted to the Lorentz component of the line shape of CO_2. In the first paper, hereafter called Part I, the half-width, its temperature dependence, and the line shift were calculated via the

* Corresponding author at: University of Massachusetts Lowell, Dept. of Environmental, Earth & Atmospheric Sciences, 1 University Avenue, Lowell, MA 01854, United States. Tel: +1 978 934 3904; fax: +1 978 934 3069.
E-mail address: Robert_Gamache@uml.edu (R.R. Gamache).

0022-4073/$ - see front matter © 2012 Elsevier Ltd. All rights reserved.
http://dx.doi.org/10.1016/j.jqsrt.2012.03.035

complex Robert–Bonamy formalism for CO_2 transitions in two of the Fermi-tetrad bands of CO_2 ($30012 \leftarrow 00001$ ($2\nu_1+2\nu_2+\nu_3$) and $30013 \leftarrow 00001$ ($\nu_1+4\nu_2+\nu_3$)) broadened by N_2 for lower rotational state quantum numbers from 0 to 120 [1]. In the second of the series, hereafter called Part II, similar calculations were carried out for O_2- and air-broadening of CO_2 [2]. In both papers comparison with measurement was made demonstrating excellent agreement; in general average percent differences of a fraction of a percent and standard deviations of ~1–2%.

Part I presented a summary of previous calculations for the half-width, line shift, and temperature dependence of the half-width by either the Anderson–Tsao–Curnutte method [3–5] or real components of Robert–Bonamy method [6]. To obtain agreement with measurements these calculations needed to introduce adjustable parameters [7,8], J-dependent scaling of the resonance functions [9], or scaled molecular parameters [7–17]. In the results presented in Parts I and II, the coefficients of the intermolecular potential (IP) that are not well known were adjusted with the goal that a single set of potential parameters would yield half-widths, their temperature dependence, and line shifts that agree well with measurement.

In this paper the studies that were done for N_2-, O_2-, and air-collisions with CO_2 are extended to the CO_2–CO_2 collision system. The calculations are made for transitions in the same spectral region as Parts I and II because of their importance to a number of measurement platforms [18–27]. Below it is shown that the results are very sensitive to intermolecular potential and that excellent agreement with experiment can be obtained from a single choice of potential parameters.

2. Complex Robert-Bonamy formalism

The calculations are a complex implementation of the semiclassical Robert–Bonamy (CRB) formalism [6], which are described in detail in Part I. Only the salient features are described here. The half-width, γ, and line shift, δ, of a ro-vibrational transition $f \leftarrow i$ are given by minus the imaginary and real parts of the diagonal elements of the complex relaxation matrix, which can be written in terms of the Liouville scattering matrix [28,29]

$$(\gamma+i\delta)_{f\leftarrow i} = \frac{n_2}{2\pi c}\sum_{J_2}\langle J_2|\rho_2|J_2\rangle \int_0^\infty vf(v)dv \times \int_0^\infty 2\pi b[1-e^{-[\mathrm{Im}(S_1+S_2)+\mathrm{Re}(S_2)]}]db \quad (1)$$

where the integration is done on the impact parameter b and the relative velocity v. ρ_2 and n_2 are the density operator and the number density of the perturber. S_1 and S_2 are the first and second order terms in the successive expansion of the Liouville scattering matrix. S_1, part of the imaginary component, is expressed in terms of the London dispersion potential [30]. S_2, a complex term, is given in terms of the electrostatic interaction potential, for CO_2–CO_2 a quadrupole–quadrupole term, and the atom–atom potential.

As demonstrated in Parts I and II, the inclusion of the imaginary terms is necessary to determine line shape parameters that satisfy the needs of the spectroscopic and remote sensing communities [31–33]. It was also shown that the expansion of the atom–atom potential must go to high *order* and *rank* in agreement with the studies of Ma et al. [34] and Gamache et al. [35]. Finally the trajectories are determined by solving Hamilton's equations using the isotropic part of the atom–atom potential. The reasons for making the calculations with these choices are explained in Parts I and II.

3. Calculations

CRB calculations were made for P- and R-branch transitions from $J''=0$ to 120 for the Fermi-tetrad bands $30012 \leftarrow 00001$ and $30013 \leftarrow 00001$ (for the notation see Part I or Ref. [36]). The calculations yield the half-width, its temperature dependence, and the line shift. The choice of these bands is that they are being used in atmospheric remote sensing measurements and that there are accurate measurements for γ, n, and δ from the work of Devi et al. [37] and Predoi-Cross et al. [17,38]. The intermolecular potential used in the calculations consist of the leading electrostatic part for the CO_2–CO_2 collision system (quadrupole–quadrupole interaction), an atom–atom part expanded to *Order* 20 and the *rank* for CO_2 set to 4, and the isotropic London dispersion vibrational dephasing term. This potential is comprised of 331 terms. Calculations were made by solving Eq. (1) doing both the integral on *db* and *dv* and using trajectories determined by solving Hamilton's Equations [39].

3.1. Initial calculations

The molecular parameters used for the initial calculations were the best available parameters reported in the literature. There are a number of measurements of the quadrupole moment of CO_2 [30]; the recommended value is that reported by Graham et al. [40], -4.017×10^{-26} esu. The static polarizability of carbon dioxide is from Bose and Cole [41], 29.13×10^{-25} cm^3, the ionization potential, 13.77 eV, is from Tanaka et al. [42]. The atom–atom constants are determined using the combination rules given in Hirschfelder et al. [43], using the homonuclear coefficients of Bouanich [44]. As discussed in Part I, within the Unsöld approximation the London dispersion potential is given in terms of the ionization potential and polarizability. For the self-collision system the static polarizability and the vibrational dependence of the polarizability of CO_2 are needed. The vibrational average value of the polarizability for a given vibrational state $|v\rangle$ is given by [45]

$$\langle v|\alpha|v\rangle = \alpha_0+a_1(n_1+1/2)+a_2(n_2+1/2)+a_3(n_3+1/2) \quad (2)$$

The coefficients for the vibrational dependence of the polarizability determined in Part I are $a_1=0.14$, $a_2=0.07$, and $a_3=0.268$. Finally the B, D, and H values used to determine the energies for CO_2 are from the work of Miller et al. [46] for the 00001 state and Devi et al. [37,47] for the 30012 and 30013 vibrational states.

Calculations of γ, n, and δ were made for P- and R-branch transitions in the $30012 \leftarrow 00001$ band for $J''=0$ to 120. In Fig. 1 the calculations are compared with the data of Devi et al. [37] and Predoi-Cross et al. [17,38]. The half-widths and line shifts show poor agreement with the

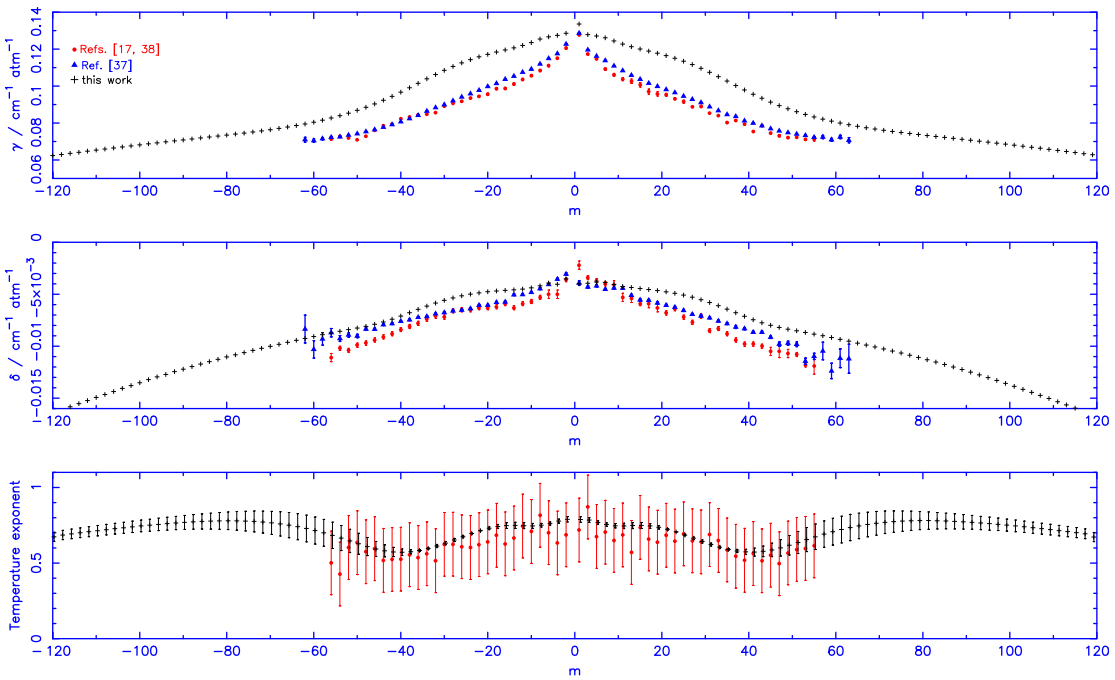

Fig. 1. CO_2–CO_2, 30012←00001 band: comparison of initial CRB calculations to the measurements of Devi et al. [37] (γ and δ) and Predoi-Cross et al. [38] (γ and δ) and [17] (n) for the half-width and line shift at T=296 K and the temperature dependence. Top panel half-widths versus m, middle panel line shifts versus m, bottom panel temperature exponent of the half-widths versus m.

measured values. As a function of m both calculated parameters have a convex structure whereas the measurements show a concave structure. The temperature dependence exponents show reasonable agreement with the measurements. This figure shows an interesting feature that for some choices of the coefficients describing the intermolecular potential one of the three parameters being fit can demonstrate good agreement whereas the others show poor to bad agreement. The hope is that only one set of potential parameters will yield all three line shape parameters agreeing with measurement.

3.2. Parameter adjustment

As in Parts I and II the goal was to find one intermolecular potential that can be used in the CRB calculations that gives results for all three parameters which simultaneously agree with measurement. The coefficients of the IP that are not well known are the coefficients for the atom–atom parameters and the parameters describing the isotropic part of the atom–atom potential that is used in the trajectory calculations, $\varepsilon_{\text{traj}}$ and σ_{traj}. A nonlinear least squares procedure was started to adjust these coefficients but it would not converge. Next, calculations were made with five percent changes individually for each IP coefficient and the change in γ, n, and δ as a function of m was plotted. From these plots and Fig. 1 the iterations continued by trial and error. Some 20 iterations later it appeared that no change would remove the convex structure of the γ and δ curves. The effect of 5% reduction in the quadrupole moment was tested, which led to a concave shape similar to the measurements. Focusing on the half-width curve, after six iterations it was found that a quadrupole moment of $\Theta = -3.698 \times 10^{-26}$ esu gave the best shape to match measurements. This value corresponds to an 8% decrease in the Graham et al. value [40]. Their determination of the quadrupole moment of CO_2 was based on 14 measurements made using a Faraday cell. Graham et al. [40] quote systematic errors of ~4% for the Faraday cell and taking 2σ uncertainty from the 14 measurements gives an error of about 7.4%. Thus the Θ value derived from our fit of the shape of the half-width curve is near the lower error estimate of Θ from the work of Graham et al. [40]. From this point on the value of the quadrupole moment used in the calculations was fixed at -3.698×10^{-26} esu. Another 50 iterations were made before the final parameters were obtained. Table 1 lists the initial and final parameters that were adjusted and the percent change. Note that the coefficients ε_{C-C} and σ_{C-C} were not adjusted since they play no role in the calculation (see Part I for

Table 1
Initial and final adjusted intermolecular potential parameters.

Parameter (units)	Initial value	Final value	% change
Θ(esu)	-4.017×10^{-26}	-3.698×10^{-26}	7.9
ε_{O-O}/k (K)	51.73	99.09	−92
σ_{O-O} (Å)	3.01	3.322	−10
ε_{O-C}/k (K)	60.55	54.47	10
σ_{O-C} (Å)	3.28	2.88	12
ε_{C-C}/k (K)	70.77	70.77	0
σ_{C-C} (Å)	3.00	3.00	0
ε_{traj}/k (K)	158.06	121.99	23
σ_{traj} (Å)	4.219	3.429	19

details). The percent changes in the atom–atom coefficients are consistent with the differences observed when different combination rules are used to determine the herero-nuclear ε and σ form homonuclear values or when homonuclear data are taken from different sources, i.e. viscosity vs. virial data ([43], and see Part I for details).

3.3. Calculations

Given the final parameters, complex (real and imaginary components) calculations were made and the half-width and line shift were determined at 13 temperatures (75, 80, 90, 100, 125, 150, 200, 250, 296, 350, 400, 500, 700 K) for all P- and R-branch transitions in the 30012←00001 and 30013←00001 bands with $J''=0$ to 120. From these data the temperature dependence of the half-width was determined in several ranges 75–700, 200–350, 125–296, and 296–700 K using the standard formula

$$\gamma(T)=\gamma(T_0)\left[\frac{T_0}{T}\right]^n \tag{3}$$

where the reference value (T_0) is taken as 296 K and n is the temperature exponent. The first range is that of the calculations, 75–750 K; the second range was made to be consistent with the measurements, 200–350 K; the third and fourth were done to be applicable to the atmospheres of Mars and Venus where self-broadening of CO_2 is important.

4. Results

The results of the calculations for the considered bands show no vibrational dependence for the half-width and the line shift, i.e. the results for the 30012←00001 and 30013←00001 bands are identical to within the uncertainty of the calculations, which is discussed below. Hence, only the calculated data for the 30012←00001 band are given in Table 2. The half-widths range from 0.0600 ($m=121$) to 0.1253 ($m=1$) $cm^{-1}\,atm^{-1}$, all the line shifts are negative and range from −0.00343 ($m=-2$) to −0.01092 ($m=121$) $cm^{-1}\,atm^{-1}$, the temperature exponents for the 200–350 K range (comparison

Table 2
Half-width, its temperature dependence, and line shift from the CRB calculations for the CO_2–CO_2 system: CO_2 transitions for $-120\le m\le 121$ in the 30012←00001 band. The half-widths and the line shifts are given in $cm^{-1}\,atm^{-1}$ at $T=296$ K.

m	γ[a]	n (125–296 K)	n (296–700 K)	δ[a]
−120	0.0602	0.770 ± 0.122	0.542 ± 0.059	−0.0103
−118	0.0604	0.766 ± 0.122	0.541 ± 0.058	−0.0103
−116	0.0606	0.764 ± 0.122	0.541 ± 0.057	−0.0102
−114	0.0609	0.761 ± 0.122	0.541 ± 0.056	−0.0102
−112	0.0611	0.757 ± 0.122	0.541 ± 0.054	−0.0102
−110	0.0614	0.755 ± 0.122	0.541 ± 0.054	−0.0101
−108	0.0616	0.752 ± 0.122	0.540 ± 0.053	−0.0101
−106	0.0618	0.749 ± 0.122	0.540 ± 0.052	−0.0100
−104	0.0621	0.746 ± 0.121	0.540 ± 0.051	−0.0100
−102	0.0623	0.743 ± 0.122	0.539 ± 0.051	−0.0100
−100	0.0626	0.741 ± 0.121	0.539 ± 0.050	−0.0099
−98	0.0629	0.740 ± 0.120	0.539 ± 0.050	−0.0099
−96	0.0632	0.738 ± 0.119	0.538 ± 0.050	−0.0098
−94	0.0634	0.733 ± 0.119	0.536 ± 0.050	−0.0098
−92	0.0637	0.732 ± 0.118	0.535 ± 0.050	−0.0098
−90	0.0639	0.729 ± 0.117	0.534 ± 0.051	−0.0098
−88	0.0642	0.727 ± 0.116	0.532 ± 0.051	−0.0097
−86	0.0645	0.724 ± 0.115	0.530 ± 0.052	−0.0097
−84	0.0648	0.722 ± 0.115	0.528 ± 0.052	−0.0097
−82	0.0651	0.720 ± 0.115	0.525 ± 0.053	−0.0096
−80	0.0654	0.718 ± 0.114	0.522 ± 0.054	−0.0096
−78	0.0657	0.716 ± 0.114	0.518 ± 0.054	−0.0095
−76	0.0660	0.713 ± 0.114	0.514 ± 0.055	−0.0095
−74	0.0664	0.710 ± 0.114	0.509 ± 0.055	−0.0094
−72	0.0667	0.707 ± 0.115	0.504 ± 0.055	−0.0094
−70	0.0671	0.703 ± 0.116	0.498 ± 0.054	−0.0093
−68	0.0675	0.698 ± 0.116	0.492 ± 0.052	−0.0092
−66	0.0680	0.693 ± 0.118	0.487 ± 0.050	−0.0091
−64	0.0685	0.687 ± 0.119	0.482 ± 0.046	−0.0091
−62	0.0690	0.680 ± 0.121	0.478 ± 0.041	−0.0089
−60	0.0696	0.672 ± 0.124	0.474 ± 0.035	−0.0088
−58	0.0703	0.663 ± 0.126	0.472 ± 0.028	−0.0087
−56	0.0711	0.652 ± 0.129	0.470 ± 0.020	−0.0086
−54	0.0720	0.641 ± 0.132	0.470 ± 0.011	−0.0084
−52	0.0730	0.629 ± 0.135	0.471 ± 0.013	−0.0083
−50	0.0741	0.615 ± 0.137	0.474 ± 0.018	−0.0081
−48	0.0753	0.601 ± 0.138	0.479 ± 0.022	−0.0079
−46	0.0767	0.588 ± 0.137	0.486 ± 0.025	−0.0077
−44	0.0782	0.573 ± 0.134	0.495 ± 0.029	−0.0075
−42	0.0798	0.560 ± 0.128	0.506 ± 0.034	−0.0073

Table 2 (*continued*)

m	γ^a	n (125–296 K)	n (296–700 K)	δ^a
−40	0.0816	0.548 ± 0.118	0.519 ± 0.037	−0.0071
−38	0.0834	0.539 ± 0.104	0.533 ± 0.037	−0.0069
−36	0.0853	0.534 ± 0.087	0.548 ± 0.036	−0.0067
−34	0.0872	0.534 ± 0.067	0.563 ± 0.032	−0.0065
−32	0.0892	0.539 ± 0.047	0.578 ± 0.026	−0.0063
−30	0.0911	0.551 ± 0.027	0.593 ± 0.019	−0.0061
−28	0.0930	0.569 ± 0.013	0.605 ± 0.010	−0.0059
−26	0.0948	0.592 ± 0.015	0.616 ± 0.005	−0.0057
−24	0.0965	0.620 ± 0.009	0.625 ± 0.010	−0.0055
−22	0.0982	0.650 ± 0.002	0.631 ± 0.016	−0.0054
−20	0.0998	0.679 ± 0.014	0.634 ± 0.022	−0.0053
−18	0.1013	0.705 ± 0.030	0.636 ± 0.025	−0.0052
−16	0.1030	0.724 ± 0.047	0.637 ± 0.025	−0.0051
−14	0.1049	0.734 ± 0.063	0.639 ± 0.020	−0.0049
−12	0.1070	0.735 ± 0.075	0.643 ± 0.014	−0.0048
−10	0.1094	0.728 ± 0.078	0.650 ± 0.008	−0.0046
−8	0.1122	0.723 ± 0.070	0.663 ± 0.004	−0.0044
−6	0.1152	0.734 ± 0.060	0.680 ± 0.006	−0.0042
−4	0.1177	0.760 ± 0.058	0.696 ± 0.012	−0.0040
−2	0.1200	0.780 ± 0.060	0.704 ± 0.016	−0.0034
1	0.1253	0.785 ± 0.061	0.706 ± 0.017	−0.0037
3	0.1187	0.771 ± 0.059	0.701 ± 0.014	−0.0036
5	0.1165	0.745 ± 0.058	0.688 ± 0.008	−0.0036
7	0.1136	0.726 ± 0.065	0.671 ± 0.004	−0.0039
9	0.1107	0.724 ± 0.075	0.656 ± 0.006	−0.0042
11	0.1081	0.732 ± 0.078	0.646 ± 0.011	−0.0045
13	0.1059	0.735 ± 0.070	0.640 ± 0.018	−0.0047
15	0.1039	0.730 ± 0.056	0.637 ± 0.023	−0.0048
17	0.1021	0.716 ± 0.038	0.636 ± 0.025	−0.0050
19	0.1005	0.693 ± 0.022	0.635 ± 0.024	−0.0051
21	0.0989	0.666 ± 0.008	0.633 ± 0.019	−0.0053
23	0.0974	0.636 ± 0.005	0.628 ± 0.012	−0.0054
25	0.0957	0.607 ± 0.012	0.621 ± 0.007	−0.0056
27	0.0939	0.581 ± 0.014	0.611 ± 0.006	−0.0057
29	0.0921	0.561 ± 0.020	0.599 ± 0.015	−0.0059
31	0.0902	0.546 ± 0.038	0.586 ± 0.023	−0.0061
33	0.0882	0.538 ± 0.058	0.571 ± 0.029	−0.0064
35	0.0863	0.536 ± 0.079	0.556 ± 0.034	−0.0066
37	0.0844	0.540 ± 0.098	0.541 ± 0.036	−0.0068
39	0.0825	0.547 ± 0.113	0.527 ± 0.037	−0.0071
41	0.0807	0.557 ± 0.125	0.513 ± 0.035	−0.0073
43	0.0790	0.570 ± 0.132	0.501 ± 0.031	−0.0075
45	0.0775	0.583 ± 0.136	0.491 ± 0.026	−0.0077
47	0.0760	0.596 ± 0.138	0.483 ± 0.023	−0.0079
49	0.0747	0.609 ± 0.136	0.476 ± 0.020	−0.0081
51	0.0735	0.621 ± 0.133	0.472 ± 0.016	−0.0083
53	0.0725	0.632 ± 0.131	0.470 ± 0.011	−0.0084
55	0.0715	0.642 ± 0.127	0.469 ± 0.015	−0.0086
57	0.0706	0.650 ± 0.123	0.469 ± 0.023	−0.0087
59	0.0699	0.658 ± 0.119	0.471 ± 0.030	−0.0088
61	0.0692	0.664 ± 0.117	0.474 ± 0.036	−0.0089
63	0.0686	0.670 ± 0.114	0.477 ± 0.041	−0.0090
65	0.0680	0.675 ± 0.112	0.482 ± 0.045	−0.0091
67	0.0675	0.681 ± 0.112	0.487 ± 0.048	−0.0091
69	0.0671	0.684 ± 0.111	0.492 ± 0.050	−0.0092
71	0.0667	0.689 ± 0.111	0.497 ± 0.051	−0.0093
73	0.0663	0.692 ± 0.111	0.502 ± 0.051	−0.0094
75	0.0659	0.696 ± 0.112	0.507 ± 0.051	−0.0094
77	0.0656	0.699 ± 0.113	0.511 ± 0.051	−0.0095
79	0.0652	0.702 ± 0.113	0.515 ± 0.050	−0.0095
81	0.0649	0.705 ± 0.114	0.519 ± 0.050	−0.0096
83	0.0646	0.708 ± 0.115	0.522 ± 0.049	−0.0097
85	0.0643	0.711 ± 0.116	0.525 ± 0.048	−0.0097
87	0.0641	0.714 ± 0.117	0.527 ± 0.048	−0.0098
89	0.0638	0.717 ± 0.118	0.529 ± 0.047	−0.0098
91	0.0635	0.720 ± 0.118	0.530 ± 0.047	−0.0099
93	0.0632	0.723 ± 0.120	0.532 ± 0.047	−0.0100
95	0.0630	0.726 ± 0.120	0.533 ± 0.047	−0.0101
97	0.0627	0.729 ± 0.121	0.534 ± 0.048	−0.0101
99	0.0625	0.732 ± 0.121	0.535 ± 0.048	−0.0102

Table 2 (*continued*)

m	γ^a	n (125–296 K)	n (296–700 K)	δ^a
101	0.0622	0.736 ± 0.122	0.535 ± 0.048	−0.0103
103	0.0620	0.739 ± 0.122	0.536 ± 0.049	−0.0103
105	0.0618	0.742 ± 0.122	0.537 ± 0.050	−0.0104
107	0.0615	0.745 ± 0.122	0.537 ± 0.051	−0.0105
109	0.0613	0.748 ± 0.122	0.538 ± 0.052	−0.0105
111	0.0611	0.751 ± 0.122	0.538 ± 0.053	−0.0106
113	0.0609	0.755 ± 0.122	0.539 ± 0.054	−0.0107
115	0.0606	0.758 ± 0.121	0.539 ± 0.055	−0.0107
117	0.0604	0.761 ± 0.121	0.540 ± 0.057	−0.0108
119	0.0602	0.764 ± 0.121	0.540 ± 0.058	−0.0109
121	0.0600	0.767 ± 0.121	0.541 ± 0.059	−0.0109

[a] In units of cm^{-1} atm^{-1} at 296 K.

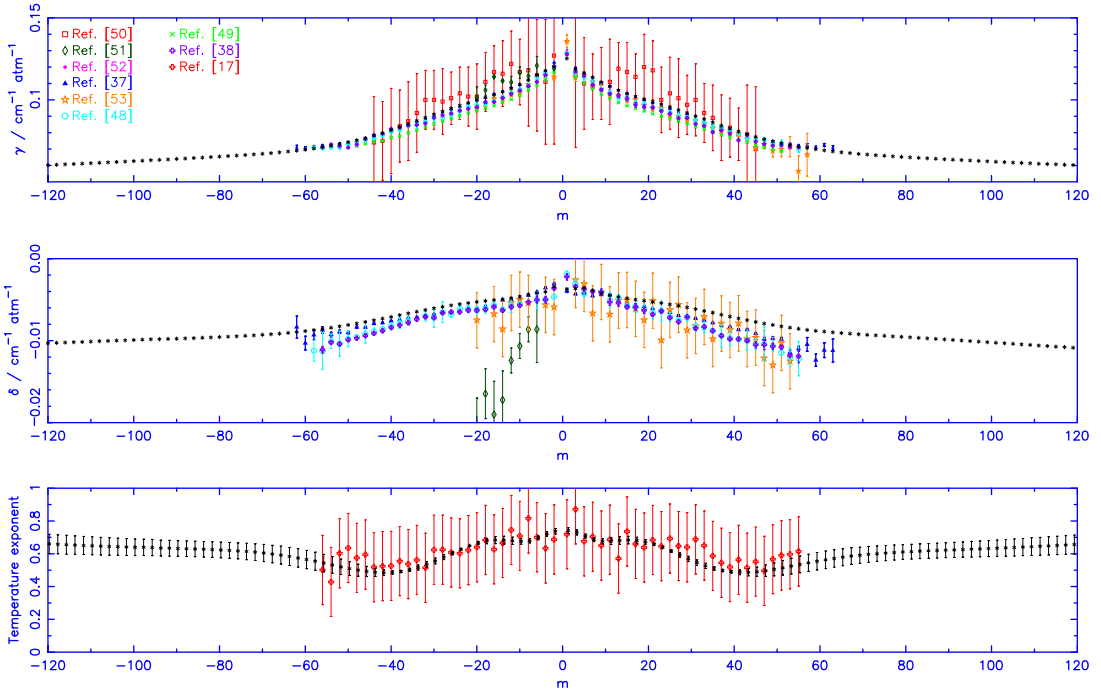

Fig. 2. Final CRB calculations for transitions in the 30012←00001 band of CO_2 broadened by CO_2 (at $T=296$ K) and measurements versus m. Top panel half-widths (in cm^{-1} atm^{-1}) versus m, middle panel line shifts (in cm^{-1} atm^{-1}) versus m, bottom panel temperature exponent of the half-widths versus m.

with measurement) are positive and range from 0.484 ($m=-42$) to 0.741 ($m=1$). In Fig. 2 the calculated data are compared to measurement. Note, all of the measurements were made within a few degrees of 296 K. The measurements are those of Devi et al. [37], Predoi-Cross et al. [38], Toth et al. [48], Régalia-Jarlot et al. [49], Valero and Suárez [50], De Rosa et al. [51], Li et al. [52], Henningsen and Simonsen [53], and Predoi-Cross et al. [17]. Before discussing the comparison of the calculations with the measurements, the agreement among the measurements will be discussed. Five of the nine references present high-resolution measurements for a large number of transitions (≥ 48) [17,37,38,48,49] (called group I below); the other 4 are a mix of high-resolution measurements of a smaller number of transitions or lower-resolution measurements of 44 transitions (called group II below). Note, all groups measured the half-width, some provide measurements of the line shift and temperature dependence of γ and/or δ. Considering the half-width and the group I references, the data of Devi et al. [37] are larger on average than the other three and the data of Régalia-Jarlot et al. [49] are the smallest on average. These two data sets are separated by roughly 7% on average. The data of Toth et al. [48] and Predoi-Cross et al. [38] are in between. The data of Henningsen and Simonsen [53] has a large spread as seen in Fig. 2, the data of Li et al. [52] is close to that of Devi et al. [37], and the data of De Rosa et al. [51] and Valero and Suárez [50] have large spread around the others.

In general the agreement of the calculations with the data is very good, the statistics of the comparisons are given in Table 3. Shown for the half-width and its temperature dependence are the average percent difference (APD) and the standard deviation of the percent

Table 3
Statistics for the comparison of the calculations to measurement.

Parameter	Ref.	# data	APD	SD
30012←00001				
γ	[50]	44	3.90	6.33
	[51]	10	3.83	3.04
	[52]	11	−0.70	1.67
	[37]	63	0.02	1.29
	[53]	38	−4.26	4.48
	[48]	56	−2.36	1.38
	[49]	49	−6.77	1.08
	[38]	56	−2.94	2.02
n	[50]	38	−30.78	70.66
	[17]	56	4.43	9.59
δ	Ref.	# data	AD[a]	$S\tilde{D}$[a]
	[51]	8	-0.939×10^{-2}	0.436×10^{-2}
	[37]	63	-0.867×10^{-3}	0.759×10^{-3}
	[48]	54	-0.142×10^{-2}	0.100×10^{-2}
	[53]	34	-0.169×10^{-2}	0.151×10^{-2}
	[38]	56	-0.140×10^{-2}	0.926×10^{-3}
30013←00001	Ref.	# data	APD	SD
γ	[57]	48	−3.93	23.41
	[47]	63	−0.27	0.99
	[48]	56	−2.43	1.35
	[49]	48	−6.44	1.38
	[56]	11	2.29	4.08
	[38]	56	−2.59	1.40
n	[57]	36	−11.29	35.05
	[17]	56	6.55	8.41
δ	Ref.	# data	AD[a]	$S\tilde{D}$[a]
	[47]	63	-0.120×10^{-2}	0.723×10^{-3}
	[48]	55	-0.166×10^{-2}	0.115×10^{-2}
	[38]	56	-0.156×10^{-2}	0.113×10^{-2}

[a] See text for definitions of AD and $S\tilde{D}$.

difference (SD). Since the magnitude of the line shifts is small a better means to compare is to use the average deviation between measurement and calculation, $AD=(\sum_{i=1}^{N}(\delta_{meas}-\delta_{calc})/N)$, rather than the percent difference. Also presented for the shifts is the standard deviation of the AD, $S\tilde{D}$. For the group I data the APDs range from −6.8 to 0.02 with the SDs that range from 1.1 to 2.0. Of the group II data, that of Li et al. [52] shows very good agreement, −0.7 APD and 1.7 SD and the other data sets displaying some scatter. The line shifts agree well with the group I data with ADs ($S\tilde{D}$) from −0.00087 to −0.0014 (0.00076 to 0.0010) cm^{-1} atm^{-1}. As can be seen in Fig. 2 the data of De Rosa et al. [51] do not agree with the other measurements or the calculations. For the temperature dependence of the half-width there are the data of Predoi-Cross et al. [17] and Valero and Suárez [50] to compare with. The calculated n values use the 200–350 K temperature range to be consistent with the measurements. The half-width data of Valero and Suárez [50] have large uncertainty and the temperature range of the study was small leading to very large uncertainty in the n values. For this reason their data were not plotted but the statistics do appear in Table 3. The agreement with the n data of Predoi-Cross et al. is good. See Table 3 for details.

The estimation of the uncertainty of the calculated parameters is difficult. Some of the intermolecular potential parameters were adjusted to fit the data of Devi et al. [37] for the half-widths and line shifts. While these data are considered "among the best" the choice of these data was because the same group had also made measurements for O_2- [54] and air-broadening [37], from which $\gamma(N_2)$ and $\delta(N_2)$ values were determined. Thus providing consistent data sets for N_2, O_2, air, and CO_2 as the buffer gas. As shown above, there are other high-resolution large data sets which differ from the Devi et al. results by ~2–6%. Each of these measurement data sets assigns the uncertainty by a $1-\sigma$ fit value, which is generally less than 1%. This uncertainty does not contain other systematic errors. Given the recent work of Birk and Wagner [55] it appears unlikely that the true error is less than 1% for the best lines, thus the uncertainty values given in Refs. [37,38,48,49] is probably best interpreted as a precision. Given that 3 of the 4 data sets are roughly within a few percent of each other, a 2% uncertainty was assigned to the data. It was also noted above that the value of the quadrupole moment of CO_2 needed to be reduced for the calculated values of the half-width to come down to the values of Devi et al., which are the largest of the group I data sets. This fact does not argue for the data of Devi et al. since the magnitude of γ may be an artifact of the calculation. However, to fit the other data sets would have required reducing $\Theta(CO_2)$ beyond the error estimate of Graham et al. [40]. Given the above, the uncertainty of the calculations should be around 2% for the half-widths and its temperature dependence and ±0.0012 cm^{-1} atm^{-1} for the line shifts.

In Fig. 3 are plotted the calculations and measurements for transitions in the 30013←00001 band in the same format as Fig. 2. The measured data are from Devi et al. [47], Toth et al. [48], Régalia-Jarlot et al. [49], Predoi-Cross et al. [38], Hikida et al. [56], Suárez and Valero [57] and Predoi-Cross et al. [17]. The features are similar to those in Fig. 2 with slightly better APDs and SDs for the half-widths but slightly larger ADs and $S\tilde{D}s$. The temperature dependence data of Suárez and Valero [57] are not plotted due to the very large uncertainty. The comparison with the measured n values of Predoi-Cross et al. [17] shows good agreement.

In parts I and II the influence of the imaginary components on the half-widths was found to be important to reach the uncertainty requirements of the remote sensing and spectroscopic communities. Here, real-component only (RRB) calculations were made and compared with the CRB calculations and it was found that the effects of the imaginary terms are less for self-broadening of CO_2 compared with N_2- or O_2-broadening. This finding is consistent with earlier studies of the effect of the imaginary components on the half-widths [58,59]. Here the maximum differences are ~3% at 75 K, 1% at 296 K to 0.5% at 700 K, which results in a maximum change in n of 2%.

There are a number of studies [60–63] that indicate the standard formula, Eq. (3), used for determining the temperature dependence of the half-width does not strictly hold for certain collision systems or over large temperature ranges. Birnbaum [64] has shown that Eq. (3) can be derived by considering a single interaction term in the intermolecular potential with all collisions being on resonance and leads to the "rule-of-thumb" formula for the temperature exponent:

$$n = (q+4)/2q \quad (4)$$

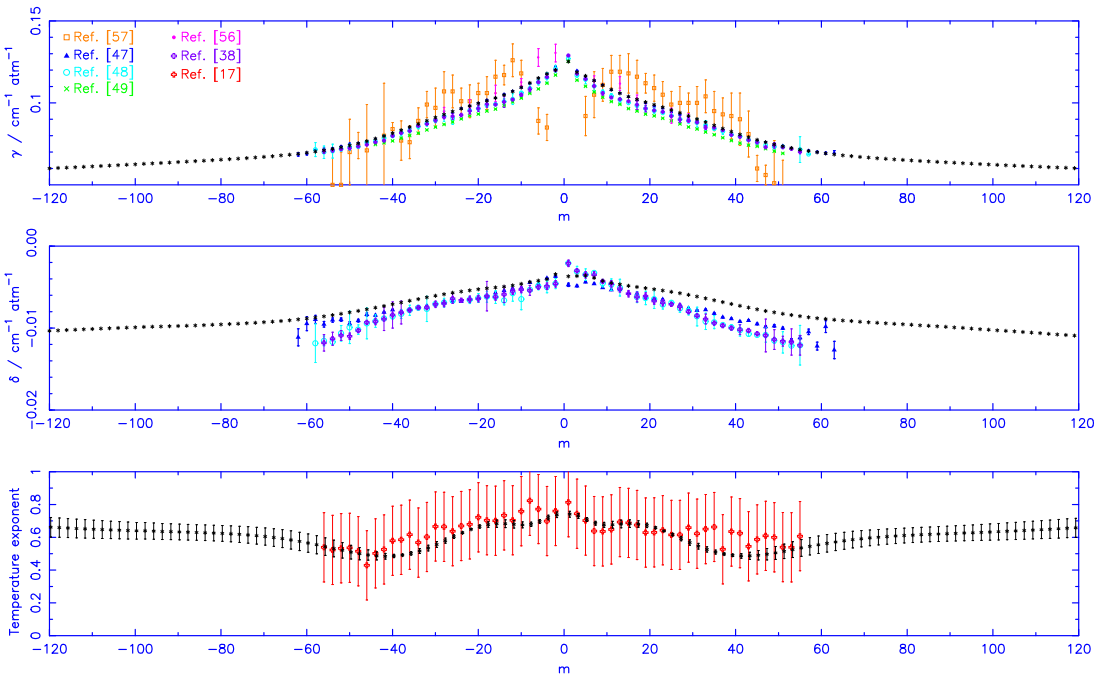

Fig. 3. Final CRB calculations for transitions in the 30013←00001 band of CO_2 broadened by CO_2 (at T=296 K) and measurements versus m. Top panel half-widths (in cm^{-1} atm^{-1}) versus m, middle panel line shifts (in cm^{-1} atm^{-1}) versus m, bottom panel temperature exponent of the half-widths versus m.

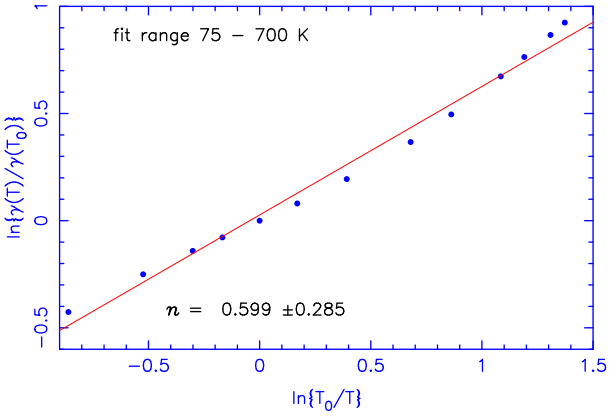

Fig. 4. Plot of $\ln[\gamma(T)/\gamma(T_0)]$ vs. $\ln[T_0/T]$ for self-broadening of the P(44) transition of CO_2 for the 30012←00001 band for the temperature range 75–700 K. Red solid line is the least-squares fit of the data points; the slope of this line is the temperature exponent. (For interpretation of the references to color in this figure legend, the reader is referred to the web version of this article).

where q=4, 6, 6, 8, 10, and 10 for dipole–dipole, dipole–quadrupole, quadrupole–dipole, quadrupole–quadrupole, dipole-induced-dipole and dispersion interactions respectively. Since the leading component of the CO_2–CO_2 system is quadrupole–quadrupole the "rule-of-thumb" value for n is 0.75. The calculations made here use an intermolecular potential comprised of 331 terms so the application of Eq. (3) as a model of the temperature dependence should be questioned. Fig. 4 is a plot of $\ln[\gamma(T)/\gamma(T_0)]$ vs. $\ln[T_0/T]$ for the temperature range 75–700 K for the P(44) transition of the 30012←00001 band. The slope of the line least-squares fitted to these points is the temperature exponent in Eq. (3); n=0.599 ± 0.285 for this transition. It is clear from Fig. 4 and the correlation coefficient (0.994) that Eq. (3) does not fit the data well for this temperature range and that choosing different temperature ranges will lead to different values of n. These results are consistent with other studies that used different temperature ranges to determine the temperature exponent [35,63,65]. For applications to planetary atmospheres a value of n determined using the temperature range of the planet's atmosphere is more appropriate. Here temperature dependence fits were made for the atmospheres of Venus (296–700 K fit range) and Mars (125–296 K fit range) where CO_2–CO_2 broadening will be important. The top panel of Fig. 5 is the result of fitting for the same transition as in Fig. 4 for the temperature range 125–296 K. The fit yields n=0.573 ± 0.134 and the fit is

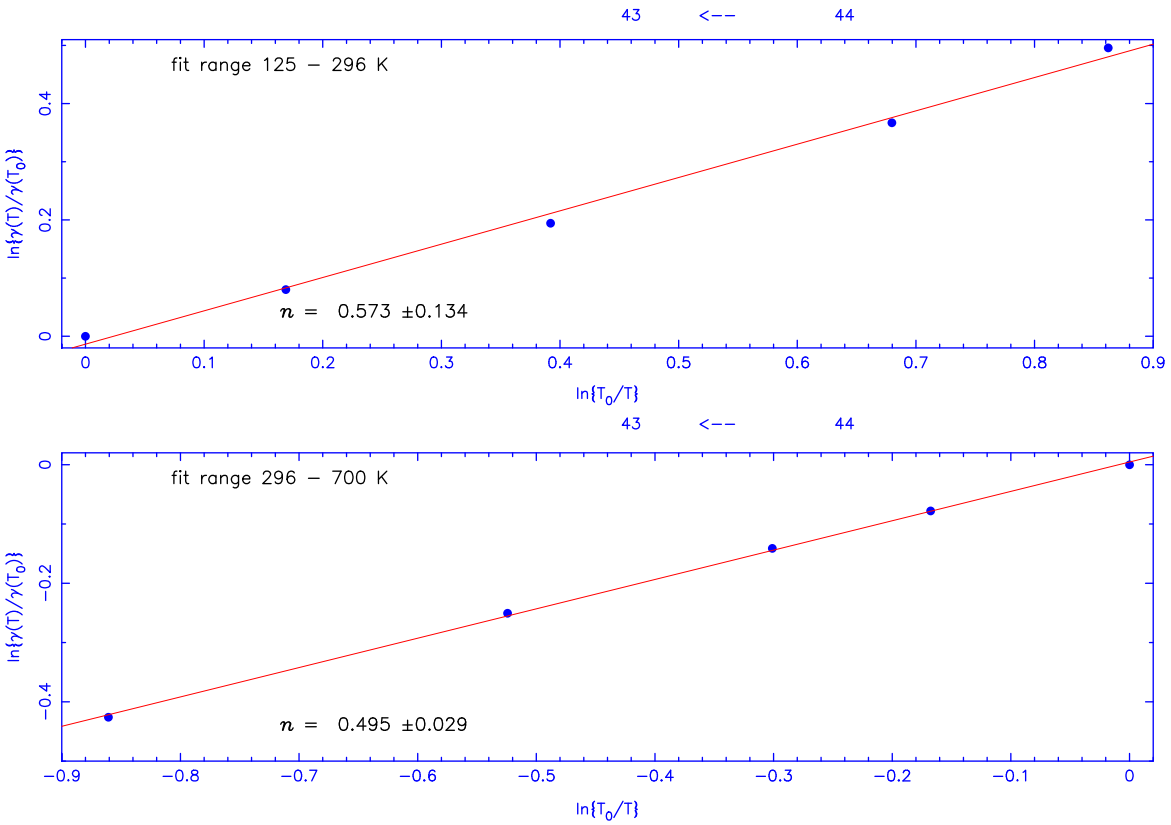

Fig. 5. Plot of $\ln[\gamma(T)/\gamma(T_0)]$ vs. $\ln[T_0/T]$ for self-broadening of the P(44) transition of CO_2 for the 30012←00001 band. Red solid line is the least-squares fit of the data points; the slope of this line is the temperature exponent. Top panel is the fit for the temperature range 125–296 K, bottom panel is the fit for the temperature range 296–700 K. (For interpretation of the references to color in this figure legend, the reader is referred to the web version of this article).

closer to the points and the correlation coefficient has improved to 0.998. This value of n is about 5% smaller than that for the 75–700 K range fit and the error is smaller by a factor of ~2. The bottom panel of Fig. 5 shows the fit for the temperature range 296–700 K. The fit gives $n=0.495\pm0.029$ and a correlation coefficient of 0.9997. This value is 21% smaller than the 75–700 K range fit and the error is smaller by more than a factor of 9. Comparing the temperature exponents from the Mars and Venus fits give an average difference of 19% with maximum differences near 29%. Table 2 contains the temperature exponents for both the 125–296 and 296–700 K fits.

5. Summary

CRB calculations for self-broadening of CO_2 were made for transitions in 2 of the Fermi tetrad bands, 30012←00001 and 30013←00001, with rotational quantum numbers from 0 to 120. The calculations used an intermolecular potential consisting of electrostatic, atom-atom (expanded to 20th order with rank 4), and London dispersion interactions. Explicit integration over the velocity was done and results reported for 13 temperatures from 75 to 700 K. The calculations included both the real and imaginary components of the S-matrices for both the half-width and line shift. The intermolecular potential (IP) was adjusted to fit measurements of the half-width, line shift, and temperature dependence of the half-width simultaneously. The results are very sensitive to the IP. It was found that the quadrupole moment of CO_2 as measured by Graham et al. [40] needed to be lowered by 8% to reproduce the shape of the measured half-width vs. m curve. Recall that the final value, $\Theta=-3.698\times10^{-26}$ esu, was used in Parts I and II of this study as well. Similar to parts I and II very few combinations of intermolecular parameters describing the IP give reasonable agreement with the three line shape parameters considered in this work. After some 70 iterations a set of IP parameters were settled upon that reproduce the measurements of Devi et al. [37].

The calculations show very little vibrational dependence, which given that the two bands are in the same polyad it is not surprising. The dependence on the imaginary components is smaller than that found in Parts I and II [1,2] but noticeable and greater than the uncertainty of the calculations for some transitions. Comparing the calculations with all measurements shows excellent agreement, in general, for the two bands that were studied.

In conclusion, the three studies, CO_2–N_2 (Part I), CO_2–O_2 and CO_2–air (Part II), and CO_2–CO_2 (this work), demonstrate that CRB calculations can use a single intermolecular potential that is expanded to high *order* and *rank,* includes the real and imaginary components, with

trajectories determined by solving Hamilton's Equations, and explicit integration over relative velocity are capable of determining the half-widths, their temperature dependence, and line shifts that are in excellent agreement with measurement. The resulting intermolecular potential will allow calculations for other vibrational bands, thus addressing more generally the dependence on vibration, as well as making line shape calculations for large values of the rotational quantum number, J'', which is important for other problems [66,67]. The databases corresponding to the data in Table 2, as well as the results for the 30013←00001 band, can be obtained at the web site of one of the authors; faculty.uml.edu/Robert_Gamache or from the supplemental information of the journal.

Acknowledgments

Some of the authors (RRG, JL, ALL) are pleased to acknowledge support of this research by the National Science Foundation through Grant no. ATM-0803135. Any opinions, findings, and conclusions or recommendations expressed in this material are those of the author(s) and do not necessarily reflect the views of the National Science Foundation. RRG and JMH are also grateful to the Paris-Est *Pôle de Recherche et d'Enseignement Supérieur* who provided a one month research scientist position for RRG at LISA in June 2011.

Appendix A. supplementary material

Supplementary data associated with this article can be found in the online version at http://dx.doi.org/10.1016/j.jqsrt.2012.03.035.

References

[1] Gamache RR, Lamouroux J, Laraia AL, Hartmann J-M, Boulet C. Semiclassical calculations of half-widths and line shifts for transitions in the 30012←00001 and 30013←00001 bands of CO_2 I: collisions with N_2. J Quant Spectrosc Radiat Transfer. http://dx.doi.org/10.1016/j.jqsrt.2012.02.014; in press.
[2] Lamouroux J, Gamache RR, Laraia AL, Hartmann J-M, Boulet C. Semiclassical calculations of half-widths and line shifts for transitions in the 30012←00001 and 30013←00001 bands of CO_2 II: collisions with O_2 and Air. J Quant Spectrosc Radiat Transfer. http://dx.doi.org/10.1016/j.jqsrt.2012.02.015; in press.
[3] Anderson PW. Dissertation physics. Harvard University; 1949.
[4] Anderson PW. Pressure broadening in the microwave and infra-red regions. Phys Rev 1949;76:647–61.
[5] Tsao CJ, Curnutte B. Line-widths of pressure-broadened spectral lines. J Quant Spectrosc Radiat Transfer 1962;2:41–91.
[6] Robert D, Bonamy J. Short range force effects in semiclassical molecular line broadening calculations. J. Phys France 1979;40:923–43.
[7] Yamamoto G, Tanaka M, Aoki T. Estimation of rotational line widths of carbon dioxide bands. J Quant Spectrosc Radiat Transfer 1969;9:371–82.
[8] Bouanich J-P, Brodbeck C. Contribution des moments octupolaire et hexadecapolaire a l'elargissement des raies spectrales de molecules lineaires. J Quant Spectrosc Radiat Transfer 1974;14:141–51.
[9] Bykov AD, Lavrentieva NN, Sinitsa LN. Calculation of CO_2 broadening and shift coefficients for high-temperature databases. Atmos Oceanic Opt 2000;13:1015–9.
[10] Arié E, Lacome N, Arcas P, Levy A. Oxygen- and air-broadened linewidths of CO_2. Appl Opt 1986;25:2584–91.
[11] Margottin-Maclou M, Dahoo P, Henry A, Valentin A, Henry L. Self-, N_2-, and O_2-broadening parameters in the ν_3 and $\nu_1+\nu_3$ bands of $^{12}C^{16}O_2$. J Mol Spectrosc 1988;131:21–35.
[12] Rosenmann L, Hartmann J-M, Perrin MY, Taine J. Collisional broadening of CO_2 IR lines. II. Calculations. J Chem Phys 1988;88:2999–3006.
[13] Rosenmann L, Perrin MY, Hartmann J-M, Taine J. Diode-laser measurements and calculations of CO_2-line-broadening by H_2O from 416 to 805 K and by N_2 from 296 to 803 K. J Quant Spectrosc Radiat Transfer 1988;40:569–76.
[14] Rosenmann L, Hartmann J-M, Perrin MY, Taine J. Accurate calculated tabulations of IR and Raman CO_2 line broadening by CO_2, H_2O, N_2, O_2 in the 300–2400-K temperature range. Appl Opt 1988;27:3902–7.
[15] Gamache RR, Rosenmann L. N_2-, O_2-, air-, and self broadening of CO_2 transitions and temperature dependence for HITRAN. Unpublished work, University of Massachusetts Lowell; 1992.
[16] Predoi-Cross A, McKellar ARW, Benner DC, Devi VM, Gamache RR, Miller CE, et al. Temperature dependences for air-broadened Lorentz half-width and pressure shift coefficients in the 30013←00001 and 30012←00001 bands of CO_2 near 1600 nm. Can J Phys 2009;87:517–35.
[17] Predoi-Cross A, Liu W, Murphy R, Povey C, Gamache RR, Laraia AL, et al. Measurement and computations for temperature dependences of self-broadened carbon dioxide transitions in the 30012←00001 and 30013←00001 bands. J Quant Spectrosc Radiat Transfer 2010;111:1065–79.
[18] Aumann HH, Gregorich D, Gaiser S. AIRS hyperspectral measurements for climate research: carbon dioxide and nitrous oxide effects. Geophys Res Lett 2005;32:L05806.
[19] Chalon G, Cayla F, Diebel D. IASI: An Advance Sounder for Operational Meteorology. In: Proceedings of the 52nd Congress of IAF, Toulouse, France; 2001.
[20] Inoue G, Yokota T, Oguma H, Higurashi A, Morino I, Aoki T.. Overview of Greenhouse Gases Observing Satellite (GOSAT) of Japan. AGU 2004 Fall Meeting, San Francisco, California, USA; 2004.
[21] Crisp D, Atlas RM, Breon F-M, Brown LR, Burrows JP, Ciais P, et al. The Orbiting Carbon Observatory (OCO) mission. Adv Space Res 2004;34:700–9.
[22] Crisp D, Miller C. The need for atmospheric carbon dioxide measurements from space: contributions from a rapid reflight of the orbiting carbon observatory. 〈http://www.nasa.gov/pdf/363474main_OCO_Reflight.pdf〉. Jet Propulsion Laboratory: Pasadena; 2009.
[23] Bovensmann H, Buchwitz M, Burrows JP, Reuter M, Krings T, Gerilowski K, et al. A remote sensing technique for global monitoring of power plant CO_2 emissions from space and related applications. Atmos Meas Tech 2010;3:781–811.
[24] Drossart P, Piccioni G, Adriani A, Angrilli F, Arnold G, Baines KH, et al. Scientific goals for the observation of Venus by VIRTIS on ESA/Venus express mission. Planet Space Sci 2007;55:1653–72.
[25] Fedorova A, Korablev O, Bertaux J-L, Rodin A, Kiselev A, Perrier S. Mars water vapor abundance from SPICAM IR spectrometer: seasonal and geographic distributions. J Geophys Res 2006;111E09S8 2006;111.
[26] McCleese DJ, Schofield JT, Taylor FW, Calcutt SB, Foote MC, Kass DM, et al. Mars Climate Sounder: an investigation of thermal and water vapor structure, dust and condensate distributions in the atmosphere, and energy balance of the polar regions. J Geophys Res 2007;112E05S6 2007;112.
[27] Wunch D, Toon GC, Blavier J-FL, Washenfelder RA, Notholt J, Connor BJ, et al. The total carbon column observing network (TCCON). Philos Trans R Soc A 2011;369:2087–112.
[28] Baranger M. General impact theory of pressure broadening. Phys Rev 1958;112:855–65.
[29] Ben-Reuven A. Spectral line shapes in gases in the binary-collision approximation. In: Prigogine I, Rice SA, editors. Adv Chem Phys. New York: Academic Press; 1975. p. 235.
[30] Gray CG, Gubbins KE. Theory of molecular fluids. Oxford: Clarendon Press; 1984.
[31] Proceedings of the Atmospheric Spectroscopy Applications Workshop, ASA REIMS 96, Université de Reims, Champagne Ardenne; 1996.
[32] Smith MAH., editor. NASA Conference Publication 2396, NASA; 1985.
[33] Smith MAH., editor. Third Langley Spectroscopic Parameters Workshop, NASA Langley Research Center, Hampton, VA; 1992.
[34] Ma Q, Tipping RH, Gamache RR. Uncertainties associated with theoretically calculated N_2-broadened half-widths of H_2O lines. Mol Phys 2010;108:2225–52.

[35] Gamache RR, Laraia AL, Half-widths Lamouroux J. their temperature dependence, and line shifts for the HDO–CO_2 system for applications to planetary atmospheres. Icarus 2011;213:720–30.
[36] Toth RA, Brown LR, Miller CE, Malathy Devi V, Benner DC. Spectroscopic database of CO_2 line parameters: 4300–7000 cm^{-1}. J Quant Spectrosc Radiat Transfer 2008;109:906–21.
[37] Devi VM, Benner DC, Brown LR, Miller CE, Toth RA. Line mixing and speed dependence in CO_2 at 6348 cm^{-1}: positions, intensities, and air- and self-broadening derived with constrained multispectrum analysis. J Mol Spectrosc 2007;242:90–117.
[38] Predoi-Cross A, Unni AV, Liu W, Schofield I, Holladay C, McKellar ARW, et al. Line shape parameters measurement and computations for self-broadened carbon dioxide transitions in the 30012←00001 and 30013 ← 00001 bands, line mixing, and speed dependence. J. Mol Spectrosc 2007;245:34–51.
[39] Lamouroux J, Gamache RR, Laraia AL, Ma Q, Tipping RH. Comparison of trajectory models in calculations of N_2-broadened half-widths and N_2-induced line shifts for the rotational band of $H_2^{16}O$ and comparison with measurements. J Quant Spectrosc Radiat Transfer. http://dx.doi.org/10.1016/j.jqsrt.2011.11.010; in press.
[40] Graham C, Pierrus J, Raab RE. Measurements of the electric quadrupole moments of CO_2, CO and N_2. Mol Phys 1989;67:939–55.
[41] Bose TK, Cole RH. Dielectric and pressure virial coefficients of imperfect gases. II. CO_2–Argon mixtures. J Chem Phys 1970;52:140–7.
[42] Tanaka Y, Jursa AS, LeBlanc FJ. Higher ionization potentials of linear triatomic molecules. I. CO_2. J Chem Phys 1960;32:1199–205.
[43] Hirschfelder JO, Curtiss CF, Bird RB. Molecular theory of gases and liquids. New York: Wiley; 1964.
[44] Bouanich J-P. Site–site Lennard–Jones potential parameters for N_2,O_2, H_2, CO and CO_2. J Quant Spectrosc Radiat Transfer 1992;47:243–50.
[45] Luo Y, Agren H, Vahtras O, Jorgensen P, Spirko V, Hettema H. Frequency-dependent polarizabilities and first hyperpolarizabilities of H_2O. J Chem Phys 1993;98:7159–64.
[46] Miller CE, Brown LR. Near infrared spectroscopy of carbon dioxide I. $^{16}O^{12}C^{16}O$ line positions. J Mol Spectrosc 2004;228:329–54.
[47] Devi VM, Benner DC, Brown LR, Miller CE, Toth RA. Line mixing and speed dependence in CO_2 at 6227.9 cm^{-1}: constrained multispectrum analysis of intensities and line shapes in the 30013←00001 band. J Mol Spectrosc 2007;245:52–80.
[48] Toth RA, Brown LR, Miller CE, Malathy Devi V, Benner DC. Self-broadened widths and shifts of $^{12}C^{16}O_2$: 4750–7000 cm^{-1}. J Mol Spectrosc 2006;239:243–71.
[49] Régalia-Jarlot L, Zéninari V, Parvitte B, Grossel A, Thomas X, von der Heyden P, et al. A complete study of the line intensities of four bands of CO_2 around 1.6 and 2.0 μm: a comparison between Fourier transform and diode laser measurements. J Quant Spectrosc Radiat Transfer 2006;101:325–38.
[50] Valero FPJ, Suárez CB. Measurement at different temperatures of absolute intensities, line half-widths, and broadening by Ar and N_2 for the 3001_{II}←0000 band of CO_2. J Quant Spectrosc Radiat Transfer 1978;19:579–90.
[51] De Rosa M, Corsi C, Gabrysch M, D'Amato F. Collisional broadening and shift of lines in the $2\nu_1+2\nu_2+\nu_3$ band of CO_2. J Quant Spectrosc Radiat Transfer 1999;61:97–104.
[52] Li JS, Liu K, Zhang WJ, Chen WD, Gao XM. Self-, N_2- and O_2-broadening coefficients for the $^{12}C^{16}O_2$ transitions near-IR measured by a diode laser photoacoustic spectrometer. J Mol Spectrosc 2008;252:9–16.
[53] Henningsen J, Simonsen H. The (2201–0000) band of CO_2 at 6348 cm^{-1}: linestrengths, broadening parameters, and pressure shifts. J Molec Spectrosc 2000;203:16–27.
[54] Devi VM, Benner DC, Miller CE, Predoi-Cross A. Lorentz half-width, pressure-induced shift and speed-dependent coefficients in oxygen-broadened CO_2 bands at 6227 and 6348 cm^{-1} using a constrained multispectrum analysis. J Quant Spectrosc Radiat Transfer 2010;111:2355–69.
[55] Birk M, Wagner G. Temperature-dependent air broadening of water in the 1250–1750 cm^{-1} range. J Quant Spectros Radiat Transfer. http://dx.doi.org/10.1016/j.jqsrt.2011.12.013; in press .
[56] Hikida T, Yamada KMT, Fukabori M, Aoki T, Watanabe T. Intensities and self-broadening coefficients of the CO_2 Ro-vibrational transitions measured by a near-IR diode laser spectrometer. J Mol Spectrosc 2005;232:202–12.
[57] Suárez CB, Valero FPJ. Intensities, self-broadening, and broadening by Ar and N_2 for the 301_{III}←000 band of CO_2 measured at different temperatures. J Mol Spectrosc 1978;71:46–63.
[58] Lynch R. Half-widths and line shifts of water vapor perturbed by both nitrogen and oxygen. PhD dissertation, Physics Department, University of Massachusetts Lowell; 1995.
[59] Gamache RR, Lynch R, Neshyba SP. New developments in the theory of pressure-broadening and pressure-shifting of spectral lines of H_2O: the complex Robert–Bonamy formalism. J Quant Spectrosc Radiat Transfer 1998;59:319–35.
[60] Wagner G, Birk M, Gamache RR, Hartmann J-M. Collisional parameters of H_2O lines: effects of temperature. J Quant Spectrosc Radiat Transfer 2005;92:211–30.
[61] Toth RA, Brown LR, Smith MAH, Malathy Devi V, Benner DC, Dulick M. Air-broadening of H_2O as a function of temperature: 696–2163 cm^{-1}. J Quant Spectrosc Radiat Transfer 2006;101:339–66.
[62] Antony BK, Neshyba S, Gamache RR. Self-broadening of water vapor transitions via the complex Robert–Bonamy theory. J Quant Spectrosc Radiat Transfer 2007;105:148–63.
[63] Gamache RR, Laraia AL. N_2-, O_2-, and air-broadened half-widths, their temperature dependence, and line shifts for the rotation band of $H_2^{16}O$. J Mol Spectrosc 2009;257:116–27.
[64] Birnbaum G. Microwave pressure broadening and its application to intermolecular forces. Adv Chem Phys 1967;12:487–548.
[65] Priem D, Colmont J-M, Rohart F, Wlodarczak G, Gamache RR. Relaxation of the 500.4 GHz line of ozone perturbed by N_2 and O_2. J Mol Spectrosc 2000;204:204–15.
[66] Lamouroux J, Tran H, Laraia AL, Gamache RR, Rothman LS, Gordon IE, et al. Updated database plus software for line-mixing in CO_2 infrared spectra and their test using laboratory spectra in the 1.5–2.3 μm region. J Quant Spectrosc Radiat Transfer 2010;111:2321–31.
[67] Rothman LS, Gordon IE, Barber RJ, Dothe H, Gamache RR, Goldman A, et al. The high-temperature molecular spectroscopic database. J Quant Spectrosc Radiat Transfer 2010;111:2139–50.